CHEMISTRY OF MATERIALS

Article

pubs.acs.org/cm

Mesoporous Hybrid Thin Film Membranes with PMETAC@Silica Architectures: Controlling Ionic Gating through the Tuning of Polyelectrolyte Density

Annette Andrieu-Brunsen,*[,†,‡] Sébastien Micoureau,[‡] Mario Tagliazucchi,[§] Igal Szleifer,[§] Omar Azzaroni,[∥] and Galo J. A. A. Soler-Illia*[,‡,⊥]

[†]Department of Chemistry, LOEWE "Soft Control", Technische Universität Darmstadt, Alarich-Weiss-Str. 4, 64287 Darmstadt, Germany

[‡]Gerencia Química, Comisión Nacional de Energía Atomica, Centro Atómico Constituyentes, Avda. Gral. Paz 1499, B1650KNA, San Martín, Buenos Aires, Argentina

[§]Department of Biomedical Engineering, Department of Chemistry and Chemistry of Life Processes Institute, Northwestern University, Evanston, Illinois 60208, United States

[∥]Instituto de Investigaciones Fisicoquímicas Teóricas y Aplicadas (INIFTA), CONICET, and Departamento de Química, Facultad de Ciencias Exactas, Universidad Nacional de La Plata, CC16, Suc. 4, La Plata, Buenos Aires, Argentina

[⊥]Departamento de Química Inorgánica, Analítica y Química Física, Facultad de Ciencias Exactas y Naturales, Universidad de Buenos Aires, Pabellón 2, Ciudad Universitaria (C1428EHA), Buenos Aires, Argentina

Supporting Information

ABSTRACT: Manipulating molecular transport through mesoporous hybrid films is a fascinating approach toward mimicking transport in nature. To understand the details in controlled transport, it is necessary to gradually adjust the charge density that in turn results in a precise adjustment of permselectivity. We have created hybrid architectures through the controlled polymerization of a strong polyelectrolyte: (2-methacryloyloxy)-ethyltrimethylammounium (PMETAC) in a mesoporous thin silica film. PMETAC contents from 5 to 100% filling can be obtained by choosing a temperature or light-induced polymerization route and by varying polymerization times, as proven by ellipsoporosimetry and infrared spectroscopy. Using cyclic voltammetry, we demonstrate that a gradual variation of ionic permselectivity from a silanol-regulated to a PMETAC-regulated permselectivity can be obtained by tuning the PMETAC mesopore filling. The resulting behavior ranges from ion exclusion to preconcentration. The experimental observations are correlated with theoretical calculations that provide quantitative insights into the organization of the ions and polymers within the pore. Our findings shed light into the understanding of the interplay between charge density and space on molecular transport, leading toward the rational design of selectively transporting synthetic membranes.

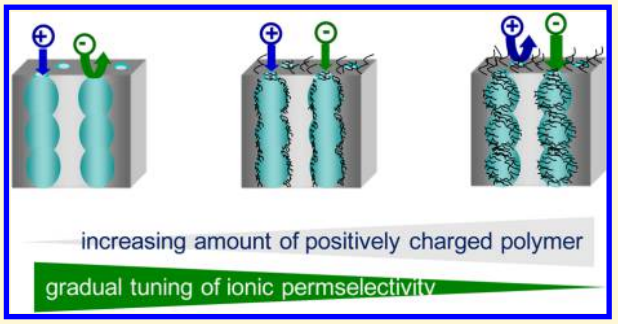

INTRODUCTION

Polymer-mesoporous hybrid materials are an exciting class of materials for a wide range of applications, from controlled release to heterogeneous catalysis or solar cells.[1−3] The charge and isoelectric point of a membrane play a key role in its mesopore accessibility, and through the control of these features, mesoporous materials are able to regulate transport of charged species. This has been widely studied in membranes for electrophoresis and related techniques and constitutes a promising basis for nanofluidics.[4] Generating hybrid mesoporous materials by surface-initiated polymerization, thus designing specifically transporting membranes, is a fascinating path toward mimicking controlled transport in nature.[5,6] A versatile route toward hybrid membranes is the use of hybrid inorganic mesoporous-polymeric films. These hybrid materials offer an independent tuning of predefined membrane structure and functionality. Switching of molecular transport through this type of materials can be achieved by inclusion of organic functions,[7−9] inclusion of charged polymers by adsorption,[10] or grafting.[11,12]

Mesoporous thin films (MTF) offer a tunable, stable, and rigid structure with pores adjustable in the range of several nanometers to hundreds of nanometers, as well as a tailorable surface chemistry that can be adjusted by designing the framework material. Furthermore, MTF can be deposited on a wide range of substrates at low temperatures and are optically

Received: October 15, 2014
Revised: December 30, 2014
Published: January 7, 2015

DOI: 10.1021/cm5037953
Chem. Mater. 2015, 27, 808−821

transparent in the visible range, allowing their integration in microelectronic or optoelectronic devices. Polymers, on the other hand, offer a great diversity of function and structure, providing the possibility to multiply functionality by controlling the degree of polymerization. For example, stimuli-responsive mesoporous systems can be designed by grafting species sensitive to physical or chemical solicitations by thoroughly controlling the mesoporous space. In the particular case of mesoporous thin films, grafting of zwitterionic polyelectrolytes leads to pH-sensitive on−off switchable hybrid membranes;[13] when phosphate-containing polymers are used as a soft building block, films can be designed to be responsive to pH or to the presence of calcium ions.[14] Light-responsive perm-selective membranes have been produced by including polymers containing photolabile groups within mesoporous silica thin films.[15,16] Thus, the combination of MTF and polymer building blocks renders functional membranes with predefined tailorable hydrophobicity, chemical stability, and catalytic or stimuli-responsive characteristics.[3,10−23]

In addition to on−off switching of transport, a gradual manipulation of transport properties would open a variety of new options from selective molecule sieving to controlled release applications. Performing controlled polymerization in nanoconfined environments permits, in principle, a precise adjustment of charge and isoelectric point, influencing transport characteristics. One possible strategy to achieve a gradual tuning of transport properties is through the control of charge density inside nanoconfined pores. The influence of polymerization parameters such as monomer concentration and polymerization time is a central issue that needs to be understood. In recent work, a gradual filling of pores with polymer has been reported.[12,24] However, no systematic way to fine-tune these features and to understand their effect on ionic permselectivity has been reported so far, even if some interesting trends regarding the important role of surface charge, type of precursors, or polymer length have been published.[10,14,15,25]

In this work we describe how to control the variation of polyelectrolyte amount in mesoporous aminosilica thin films. The charge density in the nanoconfined membrane pores was gradually adjusted by tuning the density of functional polymer in the mesopores. In this way, the ionic permselectivity of the polymer-modified mesoporous membranes was controlled. The gradual tuning of transport characteristics was achieved by varying the extent of free radical polymerization of (2-methacryloyloxy)ethyltrimethylammounium chloride (PMETAC). We explored both temperature- and light-induced polymerization methods. An appropriate choice of the polymerization method and time allows controlling the volume fraction of the polymer within the pore (pore filling, *F%*) in the 5%−100% range. These strategies enabled the gradual control of transport from exclusion to preconcentration. The experimental observations are complemented with predictions from a molecular theory that explicitly considers the polyelectrolyte chains' conformational degrees of freedom, the ions and the redox probes, the acid−base chemical equilibria, and the inter- and intramolecular interactions. The theoretical study helps to explain the molecular origin of the complex perm-selectivity behavior of the hybrid mesoporous systems.

■ MATERIALS AND METHODS

Synthesis of mesoporous aminosilica thin films. Propylamino-functionalized mesoporous thin films were synthesized, as described in previous works,[9,13,26] via the co-condensation of the oxide precursor tetraethoxysilane (TEOS, Merck) and the amine precursor 3-aminopropyltriethoxysilane (APTES, Fluka 98%) in the presence of the template (F127 block copolymer, Aldrich, M = 13600). The precursor solution was prepared using 0.8TEOS:0.2APTES:0.005F127:40EtOH:10H_2O:0.28HCl. This solution was used to produce films by dip-coating on silicon, glass, and ITO substrates under ∼40% relative humidity conditions at ∼25 °C, and 2 mm s^{-1} withdrawing speed. The organic template was removed by extraction in 0.01 moldm^{-3} HCl in absolute ethanol (Merck) for at least 3 days under stirring.

Anchoring 4,4′-azobis(4-cyanopentanoic acid) on mesoporous amino-silica films. The surface modification of the mesoporous amino-silica film with azo initiator groups was accomplished following the procedure reported by Bruening and co-workers with only minor modifications.[27] Briefly, 0.5 g (1.78 mmol) of 4,4-azobis(4-cyanopentanoic acid) and 0.92 g (4.5 mmol) of DCC were added to a single-neck Schlenk flask and closed with a rubber septum. The reactants were degassed under vacuum for 30 min followed by backfilling with $N_2(g)$. 40 mL of dry DMF were added to the flask through the septum, and the reactants were allowed to dissolve. After complete dissolution 0.13 mL of dry pyridine were added. Mesoporous films were sealed in Schlenk tubes and degassed (4x high-vacuum pump/N_2 refill cycles). The reaction mixture was syringed into the Schlenk flasks containing the mesoporous films and left overnight under $N_2(g)$ at room temperature. Finally, the mesoporous substrates were removed from the reaction mixture, immersed in a beaker containing DMF, and left over a period of 1h. The modified substrates were then washed twice with DMF followed by washing with water and ethanol. The initiator-functionalized mesoporous films were stored under nitrogen below 4 °C until further use.

Anchoring 4-Benzylbenzoic acid to mesoporous amino-silica films. The surface modification of the mesoporous amino-silica film with BP initiator groups was accomplished by the following procedure: 0.4 g (1,7 mmol) of 4-benzoylbenzoic acid and 0.92 g (4.5 mmol) of DCC were added to a single-neck Schlenk flask and closed with a rubber septum. The reactants were degassed under vacuum for 30 min followed by backfilling with $N_2(g)$. Thirty mL of dry DMF were added to the flask through the septum, and the reactants were allowed to dissolve. After complete dissolution 0.13 mL of dry pyridine were added. Mesoporous films were sealed in Schlenk tubes and degassed (4× high-vacuum pump/N_2 refill cycles). The reaction mixture was syringed into the Schlenk flasks containing the mesoporous films and left overnight under $N_2(g)$ at room temperature. Finally, the mesoporous substrates were removed from the reaction mixture, immersed in a beaker containing DMF, and left over a period of 1 h. The modified substrates were then washed twice with DMF followed by washing with water and ethanol. The initiator-functionalized mesoporous films were directly used for polymerization.

Poly(2-methacryloyloxy)ethyltrimethylammounium chloride brush growth on temperature-initiator- functionalized mesoporous silica films. In a 100 mL Schlenk flask, 23.3 g of (2-methacryloyloxy)ethyltrimethylammounium chloride as 80 wt % solution in water was added. The monomer solution was diluted with ultrapure water (Milli-Q) to 50 wt %. This solution was degassed by $N_2(g)$ bubbling for 1 h. The initiator-functionalized single mesoporous silica substrates were sealed in a Schlenk flask and degassed (4× high-vacuum pump/N_2 refill cycles). The degassed monomer solution was syringed into this Schlenk flask until all substrates were covered entirely. The flask was immersed in an oil bath preheated to 65 °C. To finish the reaction the mesoporous silica substrates were removed from the polymerization solution, washed extensively with water, and dried to yield a poly(2-methacryloyloxy) ethyltrimethylammounium chloride brush grafted mesoporous silica.

Poly(2-methacryloyloxy)ethyltrimethylammounium chloride brush growth on benzophenone light-initiator- functionalized mesoporous silica films. In a 100 mL Schlenk flask, 23.3 g of (2-methacryloyloxy)ethyltrimethylammounium chloride as 80 wt % solution in water was added. The monomer solution was diluted with ultrapure water (Milli-Q) to 50 wt %. This solution was degassed by

DOI: 10.1021/cm5037953
Chem. Mater. 2015, 27, 808−821

$N_2(g)$ bubbling for 1h. The initiator-functionalized single mesoporous silica substrates were sealed in a Schlenk flask and degassed (4x high-vacuum pump/N_2 refill cycles). The degassed monomer solution was syringed into a degassed quartz glass cuvette containing one substrate; each substrate was entirely covered. The cuvette was placed under a UV lamp at a distance of 5 cm (Philips black light, 15W, irradiation maximum at 355 nm), and irradiated for several minutes up to hours. To finish the reaction, the mesoporous silica substrates were removed from the polymerization solution, washed extensively with water, and dried to yield a poly(2-methacryloyloxy)ethyltrimethylammounium chloride brush grafted mesoporous silica.

Diffuse reflectance infrared Fourier transform spectroscopy measurements (DRIFTS) were performed on a Nicolet Magna 560 instrument, equipped with a liquid nitrogen cooled MCT-Adetector. DRIFTS measurements were performed by depositing scratched film samples on a KBr filled DRIFTS sample holder.

Small-angle X-ray scattering (SAXS). Measurements were performed at the D10A-XRD2 line of Laboratorio Nacional de Luz Síncrotron, Campinas, SP, Brazil (λ = 1.5498 Å), with a Pilatus bidimensional detector and a sample-to-detector distance of 650 mm. SAXS and Grazing-incidence SAXS (GI-SAXS) measurements were performed at 90 or 3° incidence, respectively.

Thin film characterization. Film thickness and refractive index in the 200−950 nm region were obtained using a SOPRA GES5A spectroscopic ellipsometer. Measurement of the ellipsometric parameters $\psi(\lambda)$ and $\Delta(\lambda)$ were carried out under dry nitrogen flux in order to avoid water condensation within the mesopores. The film refractive index was satisfactorily adjusted according to a one-layer model for both amino functionalized or the polymer-modified mesoporous films. A Brüggemann effective medium approximation (BEMA) was used to calculate the pore volume fraction (V_{pore}%), considering two phases made up of silica (n_{633} = 1.455) and void pores. The polymer volume fraction in the material V_{PMETAC}% was obtained by analyzing the optical data with a three component BEMA using n_{633} = 1.455 for the silica framework, n_{633} = 1.50 for PMETAC,[28] and void pores. The pore filling fraction with polymer was defined as F % = V_{PMETAC}/V_{pore}%.

Water adsorption−desorption curves (at 298 K) were measured by ellipsometric porosimetry (EP, SOPRA GES5A). Film thickness and refractive index values were obtained from measuring the ellipsometric parameters $\psi(\lambda)$ and $\Delta(\lambda)$ under nitrogen flux containing controlled water vapor quantities; P/P_0 was varied from 0 to 1 (P_0 being the saturation water vapor at 298 K). Film pore volume and pore size distribution at each P/P_0 were obtained by modeling the refractive index obtained according to a three-medium BEMA (see above) corresponding to a one layer model for the mesoporous films. Pore size distributions were obtained from the analysis of the refractive index variation along variation of water vapor pressure, using the WinElli 2 software (SOPRA, Inc.). Polymer contents (i.e., F%) were also obtained from the adsorption−desorption isotherms, by estimating the decrease in pore volume in the PMETAC-containing samples.

Cyclic voltammetry. CV was performed using a potentiostate TQ_03 with an Ag/AgCl reference electrode. All probe solutions were prepared with a concentration of 2 mM in 100 mM KCl as supporting electrolyte resulting in a pH 5−6 solution. Acidic or basic conditions (pH 3 and pH 8) were adjusted by adding a drop of a concentrated HCl or NaOH solution directly before starting the measurement. Quantitative variations in permselectivity were studied by following the changes of voltammetric peak currents associated with cationic $[Ru(NH_3)_6]^{2+/3+}$ and anionic $[Fe(CN)_6]^{4-/3-}$ redox probes, diffusing across the mesoporous film.[8]

Transmission electron microscopy (TEM). TEM measurements were made using a FEI CM20 TEM microscope with a maximum resolution of 2.3 Å, equipped with a LAB-6 cathode and a CCD camera (Olympus), using an acceleration voltage of 200 kV. Measured samples were obtained by scratching from a glass substrate. They were subsequently dispersed in some drops of ethanol. A drop of the suspension was carefully placed onto a TEM grid and ensuing solvent evaporation.

Modeling of the pore molecular organization and current of the redox probes. The concentration of the redox probe within the mesopores (C_{probe}) was calculated using a previously developed molecular theory and it was used to estimate the redox current of the probe in the cyclic voltammetry experiment under the assumption that the electrochemical response is governed by the concentration of the redox probes in the mesoporous film. The molecular theory considers explicitly the size, charge, charge distribution and conformations of all chemical species in the system, as well as the presence of coupled acid−base chemical equilibria and inter and intramolecular interactions.[29,30] In addition to the concentration of the redox probe, the theory provides us with a description of the molecular organization within the pore, namely the position-dependent concentration of all chemical species inside the pore, the electrostatic potential profile inside the pore and the degree of dissociation of the silanol and amino groups on the pore inner walls. We explain the derivation of the molecular theory and describe the molecular model used in the calculations in the Supporting Information.

■ RESULTS AND DISCUSSION

Chemistry inside nanoconfined pores demands a careful control over film and pore properties such as surface energy, charge density, functional groups, pore size, and reaction conditions, such as reactant concentration and temperature. Mesoporous aminosilica films, prepared by co-condensation, show a switch from slightly positively to negatively charged membranes around pH 3−4.[31,32] The resulting charge distribution within the pores in combination with the small pore diameter results in an exclusion of negatively charged molecules and a preconcentration of positively charged molecules at pH > 4. It has been reported that inclusion of PMETAC brushes with a polymerization degree of $N \sim 30$ inside the mesoporous aminosilica membrane leads to a completely different behavior (i.e., preconcentration of negative precursors) due to the permanent positive charges of the quaternary amino-function of PMETAC.[12] Here we present two methods that permit gradual tuning of the transport properties of hybrid mesoporous aminosilica-PMETAC membranes. This is achieved through the precise adjustment of PMETAC density that leads to a gradual adjustment of the positive charge density inside the nanoconfined pore environment, as schematized in Figure 1. Amino-silica mesoporous film matrices were produced, and an initiator for radical polymerization was grafted to the amino function (Figure 1). The polymerization routes followed involve temperature- or light-induced polymerization of $METAC^+$ monomers (see Materials and Methods for details).

Materials characterization. We used mesoporous aminosilica films produced by co-condensation (APTES:Si = 0.2:1) as a platform to build up the hybrid polymeric-inorganic membranes. Films were produced by dip-coating on silicon, glass, or indium tin oxide (ITO) substrates using Pluronics F127 block copolymer as the structure directing agent.[9,32] Films exposed to successive consolidation and extraction processes display organized pore arrays with pores having an ellipsoidal shape due to uniaxial contraction.[12]

As described in our previous works, the surface density of available amino groups for chemical reaction is highly reproducible in the range of ~16% of the total population of amine groups.[12,32] These functional groups were used as grafting sites for the surface-initiated free radical polymerization of poly 2-(methacryloyloxy)ethyltrimethylammonium chloride) (PMETAC) brushes. In a first step the amino groups were conjugated to two different surface-confined initiators: 4,4′-azobis(4-cyanopentanoic acid) (ACVA) or 4-benzoylbenzoic acid (BP) as temperature[27] or light-initiators, respectively.

DOI: 10.1021/cm5037953
Chem. Mater. 2015, 27, 808−821

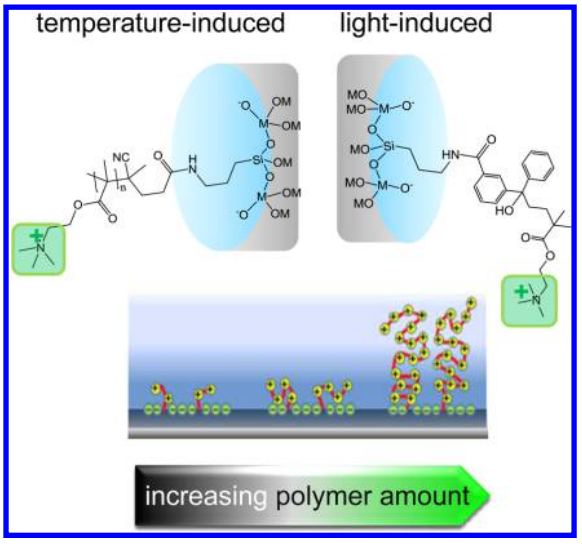

Figure 1. Schematic depiction of the two routes (thermal- and light-induced) with different initiators explored for reaction-time dependent adjustment of PMETAC function density in mesoporous aminosilica films. The transport regulating variables are linked with the ability of adjusting polymerization time and type of polymerization on the amount of permanently positively charged PMETAC brushes, and tuning the polymer interaction with the silanol surface groups that define the pore charge.

Subsequently, brush polymerization was accomplished by surface-initiated free radical polymerization of METAC monomers in the presence of water as solvent. Interestingly, under these conditions, the aminosilica walls should be charged negatively, causing a preconcentration of the METAC monomers inside the pores, thus favoring the reaction to proceed within the mesopore volume.[12] A representative transmission electron microscope (TEM) image of a scratched film and a 2D SAXS pattern in which an ellipse and reinforcements corresponding to cubic mesostructure can be observed are presented in Figure 2.

Qualitative characterization of polymer-containing mesoporous films. In order to manipulate the polymer content and thus the charge density, polymerization time was varied between minutes up to several hours. The presence of PMETAC was confirmed by Diffuse Infrared Fourier Transform Spectroscopy (DRIFTS). Figure 3 depicts the DRIFT spectra after temperature-induced (Figure 3A) and photo-induced polymerization of PMETAC (Figure 3B). The bands corresponding to the inorganic matrix, such as the Si−OH and Si−O−Si stretching at ∼966 and ∼1080 cm^{-1}, do not change significantly upon polymerization. Additionally, characteristic bands corresponding to the N−H asymmetric bending of the amine group around ∼1560 cm^{-1} can be identified. Upon polymer modification, a C═O stretching bond at ∼1727 cm^{-1} appears. This band can be attributed to the ester linkage of METAC monomer units in the PMETAC polymer backbone. This C═O stretching signal increases with increasing ratio of PMETAC per amount of silica.

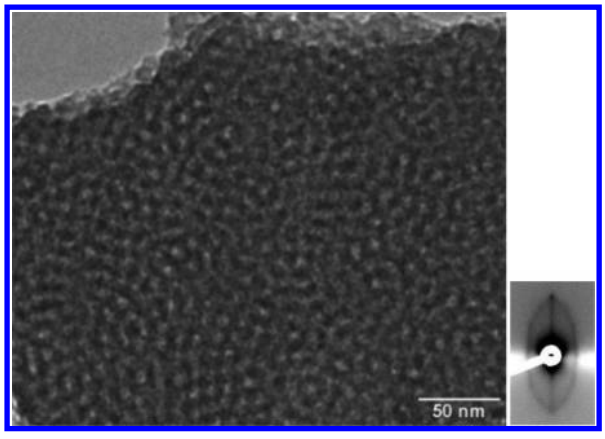

Figure 2. Representative TEM image (left) and 2D-SAXS transmission pattern obtained at 3° incidence (right) of aminopropyltriethoxysilane (APTES)-functionalized mesoporous silica thin films ($NH_2(CH_2)_3Si$ function) with a molar ratio of co-condensed APTES of 20 mol %, after treatment to 200 °C and template extraction.

Figure 3A shows a selected region of the DRIFTS spectrum of an amino-silica film obtained by temperature-induced polymerization, normalized to the δ_{H2O} bending signal at 1670 cm^{-1}. Spectra also display the bands corresponding to the characteristic N−H asymmetric bending of the amine group around ∼1560 cm^{-1} and the C═O stretching bond at ∼1727 cm^{-1} that appears upon polymer modification. Two temperature-induced polymerization times of 40 (cyan, dashed trace) and 210 min (blue, solid line) are compared to the original amino-functionalized film (black full line). The C═O stretching band at ∼1727 cm^{-1} increases from 0 to 210 min polymerization time. However, the signal is small, indicating a low amount of PMETAC.

Light-induced polymerization, with benzophenone as a type II photoinitiator, leads to much higher overall polymer content, as well as a faster polymerization with respect to overall reaction time and achieved polymer amount under the applied experimental conditions (Figure 3B). Figure 3B depicts representative DRIFT spectra, which are normalized to the asymmetric Si−O−Si stretching signal at ∼1080 cm^{-1}. These spectra show considerably higher C═O vibrational bands, markedly increasing with polymerization time. It is important to recall that both initiation mechanisms are dissimilar and that different initiation efficiency is expected due to the differences in the initiator molecules and energy supply (i.e., themal versus photoinitiation). ACVA as a temperature initiator decomposes into two identical radicals, one bound to the surface and one being liberated into solution, whereas benzophenone initially generates a surface bound biradical which is able to remove a proton from C−H bonds. Under the applied experimental conditions, benzophenone seems to be more efficient to generate polymer. In all our experiments a significantly higher amount of PMETAC was generated by using benzophenone as photoinitiator compared to ACVA as thermal initiator.

The presence of initiator and PMETAC in the mesoporous membrane also causes an appreciable increase in the contact angle, from *ca.* 25° in the amino functionalized films to 60−80° after initiator binding and extensive polymerization. This increase in contact angle is another proof that surface functionalization took place.

Estimation of polymer contents. Previous works have assessed that, in the co-condensation synthetic conditions used in this paper, ∼16% of the amino groups are available for reaction at the mesopore surface. This results in an approximate ratio of available amino to silanol of -NH_2:-OH ∼ 1:4.[12,25,32] In this framework, the pore should be overall neutral for a polymerization degree of PMETAC of N = 4, assuming that all amino groups carry an initiator and all initiators identically initiate a polymerization. Based on these assumptions, the

DOI: 10.1021/cm5037953
Chem. Mater. 2015, 27, 808−821

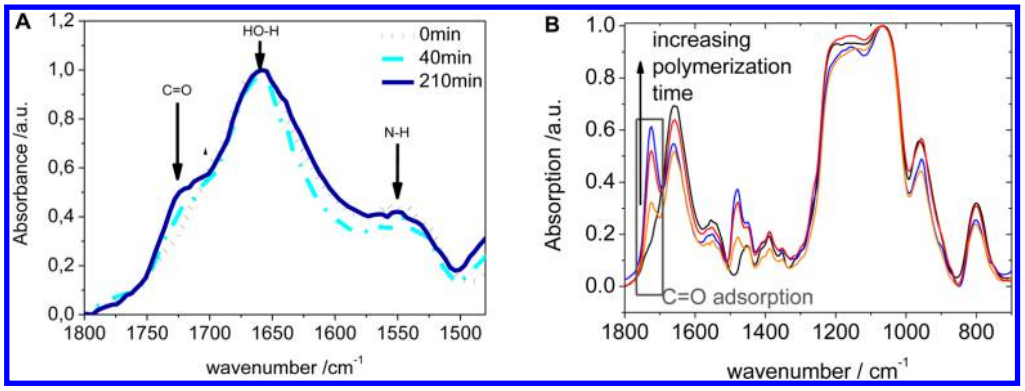

Figure 3. DRIFT spectra in dependence of the polymerization time for temperature-induced polymerization with ACVA (A) and light-induced polymerization with BP (B) (black, 0 min; orange, 5 min; red, 10 min; blue, 2 h). The ester-carbonyl band at 1727 cm^{-1} reflects the increasing PMETAC content with increasing polymerization time. The much higher PMETAC content upon photopolymerization for comparable reaction times is clearly visible.

amount of monomers per amino group ($n_{METAC}/n_{NH2'}$) can be calculated by normalizing to the equivalent intensity of surface amino groups that should have reacted ($0.16I_{SA}$) as expressed in the following equation:

$$n_{METAC}/n_{NH_2} = \frac{\varepsilon_{PMETAC}(I_{PMETAC} - I_0)}{0.16(\varepsilon_{SA}I_{SA})} \quad (1)$$

with I_{PMETAC} being the absorption of the $I_{C=O}$ band in the DRIFT spectra at 1727 cm^{-1}, I_{SA} referring to the DRIFT absorption of the amino groups at 1560 cm^{-1} multiplied by the ratio of reactive surface amino groups (16%), and I_0 referring to the baseline at the position of the C═O band at 1727 cm^{-1}. The measured signal intensity has to be corrected by the absorption coefficient (ε). Referring to literature values, typical values for ε(C═O) are in the range of 260−450, whereas values for $\varepsilon(NH_2)$ are in the range of 60−150.[33] This results in a factor of 2−3 comparing both absorbances. Using an approximate average ratio ε(C═O)/$\varepsilon(NH_2) \sim 3$, the number of monomers per surface amino function obtained from the DRIFTS can be estimated as $n_{METAC}/n_{NH2} \sim 1.2$ after 40 min and $n_{METAC}/n_{NH2} \sim 2.3$ after 210 min of temperature-induced polymerization using ACVA (Table 1). This implies a change in the pores surface charge after temperature-induced polymerization, and a pore volume filling of ∼7−8% consistent with the EP results as discussed below.

In the case of light-induced free radical polymerization with a benzophenone initiator, a much higher pore filling degree is obtained in shorter reaction times. An estimation of the polymer contents derived from the IR data under the same assumptions discussed above (eq 1) leads to significantly higher n_{METAC}/n_{NH2} values. The absolute values might vary due to the error introduced by the uncertainty of the absorption coefficient (ε) ratio between C═O of the PMETAC and the amino group, but the relationship between the polymer contents along different polymerization times should not be greatly affected. Taking into account an approximate (reactive amino):(surface silanolate) ratio of 1:4, an already slightly positively charged membrane can be obtained even after a short irradiation period of 10 min. Interpreting this data, one has to be aware that polymerization was performed inside the mesopores, but can also take place on the outer film surface. Consequently, the mentioned values are mean values for both polymer locations. Additionally, we performed free radical polymerizations that should not produce well-defined polymer brushes, and branching is very likely to occur. Thus, the values for n_{METAC}/n_{NH2} reported here are meant as an average number of charge carrying monomers per initial amino surface group, and not as the actual degree of polymerization.

Additionally, an analysis of polymer content and pore filling was performed by using ellipsometry under dry nitrogen flux (i.e., 0% humidity) and ellipsoporosimetry (EP). The results are gathered in Table 1. Ellipsometric analysis of mesoporous films prior to and after polymerization of PMETAC was performed for films submitted to varying humidity between 0% and 100%. The obtained ellipsometric parameters $\Psi(\lambda)$ and $\Delta(\lambda)$ were satisfactorily adjusted between 300 and 900 nm using a single layer model. The pore volume fraction (V_{pore}%) in mesoporous empty or polymer-loaded films was assigned using a BEMA model. Water adsorption−desorption isotherms obtained from EP measurements are shown in Figure 4. In all cases, type IV isotherms are obtained, presenting H2 hysteresis loops. Pore volume can also be extracted from the isotherms, as well as the pore and neck size distributions, according to the model proposed by Boissière et al. for ellipsoidal mesopores.[34] One has to mention that EP measurements reflect the interactions of water and the oxide surface; thus, a change in contact angle strongly influences the obtained pore diameter, but not the refractive index, the thickness, or the shape of the sorption isotherms. By comparing the adsorption−desorption isotherms for ACVA- (Figure 4 A) and benzophenone-initiated METAC polymerization (Figure 4B), the different degrees of pore filling are directly visible.

Table 1. Pore Filling with Increasing Polymerization Time Measured by Different Characterization Techniques

Time/ min	$n_{633\ (0\%)}$	CA/ deg	$V_{pore\%\ (EP)}$	d_{pore}/ nm	d_{neck}/ nm	F% (EP)	n_{METAC}/n_{NH2}*
***T*-Induced Polymerization**							
0	1.300	26	31	8.2	3.5	0	0
40	1.313	30	30	6.8	3.3	4	1.2
120	1.338	61	28	4.6	2.8	11	-
210	1.340	61	24	4.6	2.6	23	2.3
Light-Induced Polymerization							
0	1.307	25	30	7.8	3.5	0	0
10	1.374	80	16	4.5	2.6	47	5.6
30	1.401	80	11	3.2	2.1	63	9.2
120	1.468	80	0	0	0	100	15

*Polymerization degree, estimated by DRIFTS; see text.

DOI: 10.1021/cm5037953
Chem. Mater. 2015, 27, 808−821

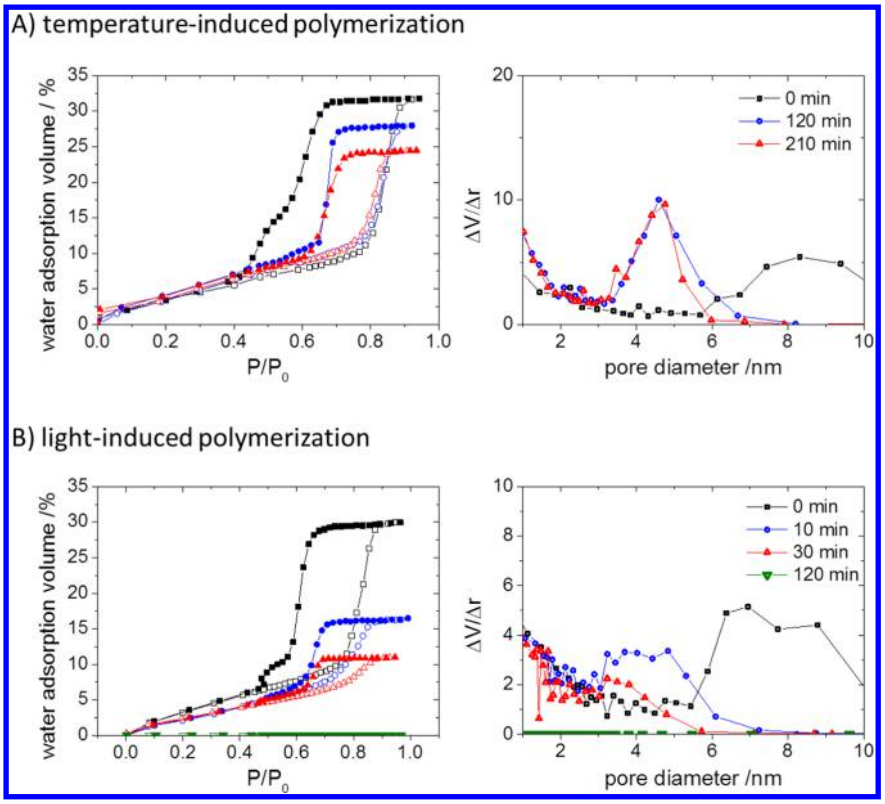

Figure 4. Water adsorption isotherms (left) and pore size distributions (right) as determined from the adsorption branch in EP upon increasing polymerization time of PMETAC brushes for temperature-induced (a, black: 0 min, orange: 40 min, blue: 2 h, red: 3.5 h) and light-induced (b, black: 0 min, blue: 10 min, red: 30 min, green: 120 min) free radical polymerization.

For an amino-modified silica film, an average pore volume fraction (V_{pore}%) of 33 ± 2% was calculated from the refractive index at 0% humidity applying BEMA (see Materials and Methods for details). This pore volume is in excellent agreement with the pore volume fraction of 31 ± 1% found by analyzing the water adsorption−desorption isotherms obtained by EP. Pore size distributions centered with an average pore diameter of 8.2 nm and a neck size of 3.5 nm diameter were calculated from the adsorption and desorption branches of different samples, respectively.

The EP water isotherms of Figure 4 show a general trend. First, a consistent decrease in V_{pore}% and pore diameter is observed for longer polymerization intervals, indicating polymer incorporation into the pore system along reaction time for systems submitted to thermal or photoinitiated polymerization. Coincidently, pore diameters decrease upon polymerization. In addition, by comparing the water adsorption, the pore volume, and the resulting pore size distribution, it can be immediately observed that the thermal-induced pathway (Figure 4A) leads to a significantly lower polymer inclusion than the light-induced one (Figure 4B), in excellent agreement with the FTIR information. The pore volume fraction filled with polymer *F*%, and the pore and neck diameter obtained from EP measurements for the different times and polymerization routes are detailed in Table 1.

In the case of temperature-induced free radical polymerization, a large fraction of the pore volume remains accessible for water adsorption even after 210 min of reaction. An increase in *F*% is observed along the polymerization reaction, reaching approximately a value of *F*% = 23% for samples submitted to 210 min polymerization time due to the gradual growth of PMETAC within the mesopores. At this point, the estimated n_{METAC}/n_{NH2} = 2.3 according to DRIFT results. Pore and neck sizes obtained from EP (Table 1) show a size reduction from 8.2 to 4.6 nm, and from 3.5 to 2.6 nm, respectively.[35] This reduction of the pore diameter of ∼3.6 nm for relatively short polymers (n = 2.3) is in agreement with what would be expected. Using a roughly estimated volume of 0.262 nm^3 for a METAC monomer (from the van der Waals radii, see below) and a grafting density of 0.9 amino groups per square nanometer according to the estimation of active amino groups and the total number of 4.5 silanolate groups per square nanometer,[36] a more or less close packed polymer with n_{METAC}/n_{NH2} = 2.3 would lead to ca. 6.3 nm diameter. Film thicknesses of 2 nm were reported for brush layers synthesized by ATRP without blocking nanopores with a diameter in the range of 22 nm,[24,37,38] which is larger than the here reported pore sizes. An estimation using the C−C bond length would yield approximately $n_{METAC}/n_{NH2} \sim 3$ for a reduction of pore radius of ∼1.5 nm, again leading to ∼5.2 nm diameter. The observed differences are in this scenario lie within reasonable uncertainties due to the different techniques and models used in such complex systems.

In the case of light-induced free radical polymerization with a benzophenone initiator, a much higher pore filling degree is obtained in shorter reaction times. Indeed, complete pore blocking for water adsorption is obtained after 120 min irradiation (Figure 4d−f), as indicated by the high value of n_{633} = 1.467 at 0% humidity, for a sample obtained after 120 min of light-induced polymerization. Coincidently, the pore diameters obtained by the Kelvin equation significantly decrease upon polymerization even after short irradiation times, until pores seem to be inaccessible to water (Figure 4f) after 120 min of irradiation (Table 1). This behavior is in contrast to the

DOI: 10.1021/cm5037953
Chem. Mater. 2015, 27, 808−821

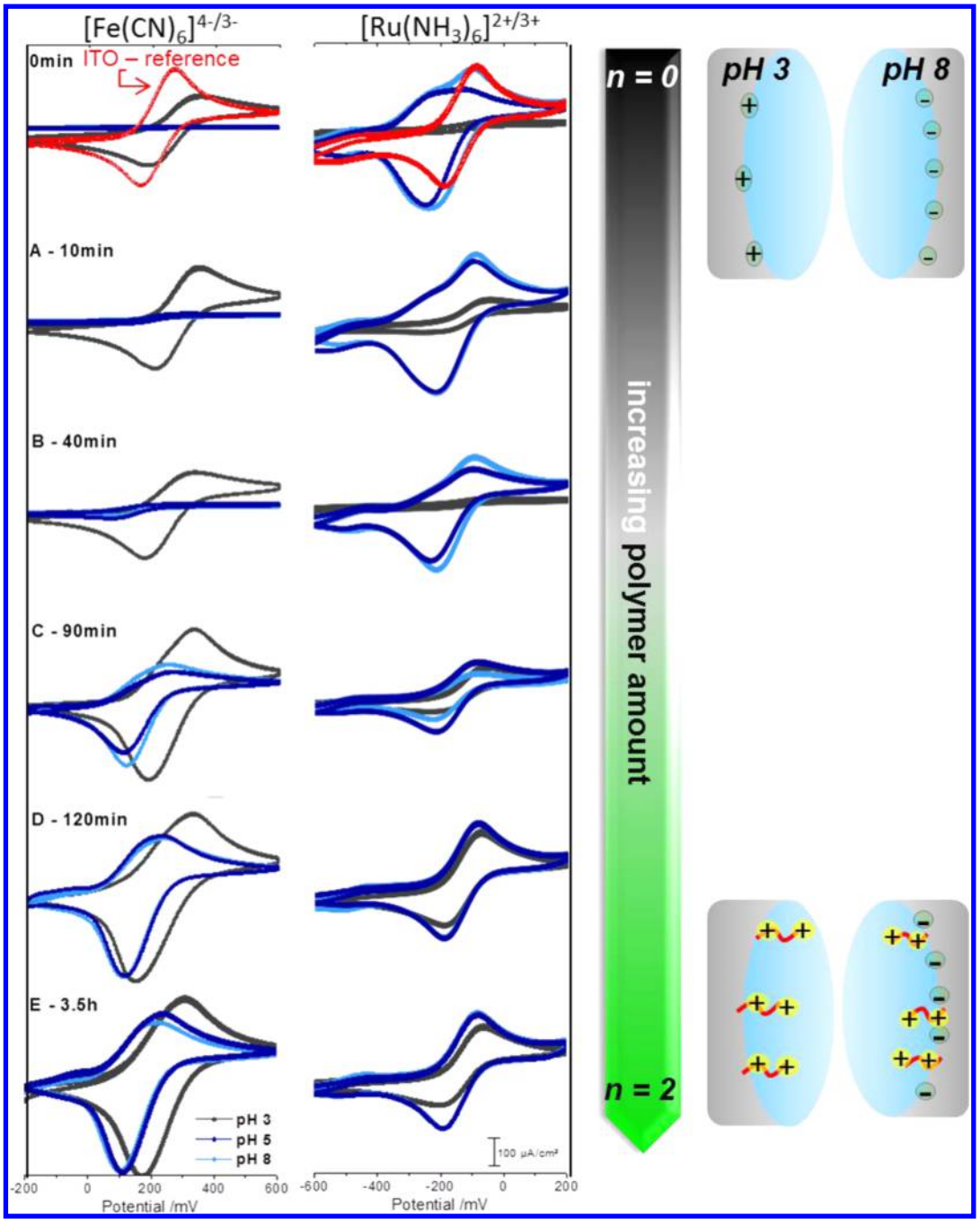

Figure 5. Cyclic voltammetry response for the charged probes $[Fe(CN)_6]^{4-/3-}$ (left) and $[Ru(NH_3)_6]^{2+/3+}$ (right) in dependence of polymerization time (0 min; A, 10 min; B, 40 min; C, 90 min; D, 2 h; E, 3.5 h) and pH (gray, pH 3; blue, pH 5; light blue, pH 8), for the temperature-induced polymerization. The red trace in the first graph for 0 min corresponds to the response of the probe solution on the bare ITO electrode.

temperature-induced polymerization that only led to a very low amount of pore filling up to 210 min of reaction.

In summary, the maximum pore filling that could be achieved here by temperature-initiated polymerization is roughly comparable to the lowest polymer filling achieved by light-induced polymerization. Both methods are complementary and allow a gradual tuning of polymer amount. While light-induced polymerization leads to water-inaccessible mesopores in short times, the thermal initiator method can be used to fine-tune low loadings of functional monomers. It is also clear that a set of different techniques such as EP and DRIFTS is necessary to estimate the pore filling. Slightly different absolute values were obtained with different characterization methods due to different limitations and different models to interpret pore filling. However, both methods overall coincide in the general trend. This permits association with the amount of charged monomers per amino group (n_{METAC}/n_{NH2}) in the mesoporous film to our ionic permselectivity, which will be discussed in the next section.

Transport characteristics. Transport of molecules along mesoporous systems is governed by the complex interplay between diffusion and adsorption kinetics on the pore surface.[39,40] A delicate balance is set between diffusion and adsorption controlled processes, which crucially depends on the pore dimensions, as well as the nature and availability of surface sites, and their charge speciation. In particular, the accurate

DOI: 10.1021/cm5037953
Chem. Mater. 2015, 27, 808–821

control of the pore surface charge density is crucial to design ion selective transport systems, to tailor transport manipulation through nanoconfined pores, as well as to exploit preconcentration phenomena. The understanding of these effects permits creation of specific systems in applications such as catalysis, membranes, or drug delivery.[44]

Adsorption of the positively charged fluorescent dye Rhodamine B in PMETAC-modified films obtained by photopolymerization showed a clear decrease of fluorescence intensity with increasing polymer content (Figure S1). This suggests that a gradual charge density variation is achieved that changes the electrostatic-driven adsorption of the charged dyes. In order to shed light on the perm-selective properties and perform a more quantitative analysis, cyclic voltammetry (CV) was used. This technique is currently used in the recent literature to investigate the influence of charge on the transport properties of charged probe molecules in mesoporous materials. The detailed response of CV probed in mesoporous materials depends on complex processes that are not yet fully understood, and the current density obtained under diffusion-limited conditions is related to a combination of the electrochemical probe concentration as well as its diffusion rate.[41] However, it is well-known that the change in voltammetric response of mesoporous electrodes reflects the variation in the probe accessibility with the architecture and the electrostatic environment of the nanoconfined pores. Well-ordered mesostructures can display enhanced transport properties of guest-molecules compared to nonmesostructured architectures.[31,42] For example, recent work by Walcarius et al. shows an enhancement of the voltammetric signal of 1 order of magnitude in the case of a mesoporous film deposited onto an ITO electrode compared to a bare ITO surface.[43] As recently demonstrated, pore filling of mesoporous films of about 83% with PMETAC leads to an inversion of charge from a pH-switchable, negatively charged or neutral mesoporous film to a permanently positively charged PMETAC-modified mesoporous film.[12] This permanent positive charge causes a preconcentration of negatively charged molecules and thus a significant voltammetric signal enhancement, whereas positively charged molecules are excluded. This effect was used to generate metallic nanoparticles through electrostatic precursor preconcentration.[12,44] In this context, it is of particular importance to understand the effect of the polymer length on the generation of pores with intermediate charge states that can display tunable transport properties.

The influence of polymer contents in the transport properties of the PMETAC-containing mesoporous aminosilica thin films for the two different initiation systems was analyzed. Ferrocyanide (***FC***, $[(Fe(CN)_6]^{3-}$) and hexaaminoruthenium (***RA***, $[Ru(NH_3)_6]^{3+}$) were used as negatively or positively charged probe molecules respectively, to investigate PMETAC-functionalized mesopore permselectivity. CV measurements were performed at pH values of 3, 5, and 8. It is important to note that a combined effect of the pore wall and the polyelectrolyte charges is expected through all the pH range. Aminosilica mesoporous film walls bear a slightly positive charge at pH of 3 whereas they are negatively charged at pH > 4.5, due to deprotonation of the surface silanol groups,[45] while the PMETAC chains introduce a permanent positive charge. In principle, transport properties can be adjusted by controlling intrinsic (polymer length) or extrinsic (pH, ionic force, counterions) conditions but especially at low PMETAC contents, the system becomes quite complex due to the confined charges.[46]

Temperature-induced polymerization. Figure 5 shows measured cyclic voltammogramms (CV) for the charged probes ***FC*** and ***RA*** in films presenting varying degree of pore filling after thermally induced polymerization using ACVA. Curves correspond to anionic ***FC*** (left) and cationic ***RA*** (right), at pH values of 3 (gray), 5 (blue) and 8 (light blue). It is worth noting that in all cases the peak currents increase as $v^{1/2}$ (see Figure S2), indicating that the electrochemical response is limited by diffusional charge transport rather than by interfacial charge transfer.

At a first glance, the positive and negative probes show different behavior: a significant effect of the introduced number of monomers, n_{METAC}/n_{NH2}, and pH in the CV signals is observed, demonstrating the important role of the surface charge in the charge transport, in agreement with observations from previous works.[4,43,47] It has to be recalled from the previous section that thermal initiation leads to low PMETAC charges, i.e., $n_{METAC}/n_{NH2} < 3$, and that pH variation influences the charge of the silica wall, but not the positive charge of the polymer.

For unmodified films ($n_{METAC}/n_{NH2} = 0$), the observed peak current density (j_p) of the anionic probe ***FC*** is always lower compared to the one of bare ITO, with a maximum current density at pH of 3 (Figure 5, 0 min). The lower current observed in the mesoporous membrane-initiated film with respect to bare ITO results from a balance between a lower available electrode area, a high pore accessibility, and some preconcentration effect.[48] No appreciable current can be observed in the ***FC*** voltammetry for pH > 5 due to the negatively charged silanolate groups. In contrast, the positively charged ***RA*** probe presents no signal at a pH of 3. At higher pH values, the ***RA*** probe presents a higher signal with respect to the current of bare ITO for the same probe solution (Figure 5, 0 min). For aminosilica and low PMETAC content samples, we observe two anodic peaks located at ~ -80 and -195 mV, while for bare ITO or samples with large PMETAC content we observe only the peak at -80 mV. A possible explanation is that the signal at -80 mV corresponds to the signal of free ***RA*** probes, while the anodic peak at ~ -195 mV corresponds to ***RA*** cations electrostatically adsorbed to free silanolate groups. In the latter case, electron transport might be due to electron hopping along surface adsorbed species.

The voltammograms in the presence of FC show increasing broadening as the polymer content increases, although there is always only one anodic and one cathodic peak. Peak broadening is indicative of redox probes in different molecular environments (which have different apparent redox potentials and/or mobilities). We propose that the broadening in the case of FC is due to the electrostatic association of the FC anion with the PMETAC polycation.

The global behavior for both probe molecules indicates that the surface charge of aminosilica films ($n_{METAC}/n_{NH2} = 0$) is dominated by the negatively charged silanolate groups present on the wall surface at pH > 4.5 and protonated amino groups for acidic pH. The resulting electrostatic effects are responsible for the exclusion or preconcentration of both probes. The pH dependence of the transport of both the positive and negative probes in the blank systems is in line with previous works indicating that the amino-silica pore bears a positive charge at low pH due to the presence of propylammonium and silanols;

DOI: 10.1021/cm5037953
Chem. Mater. 2015, 27, 808−821

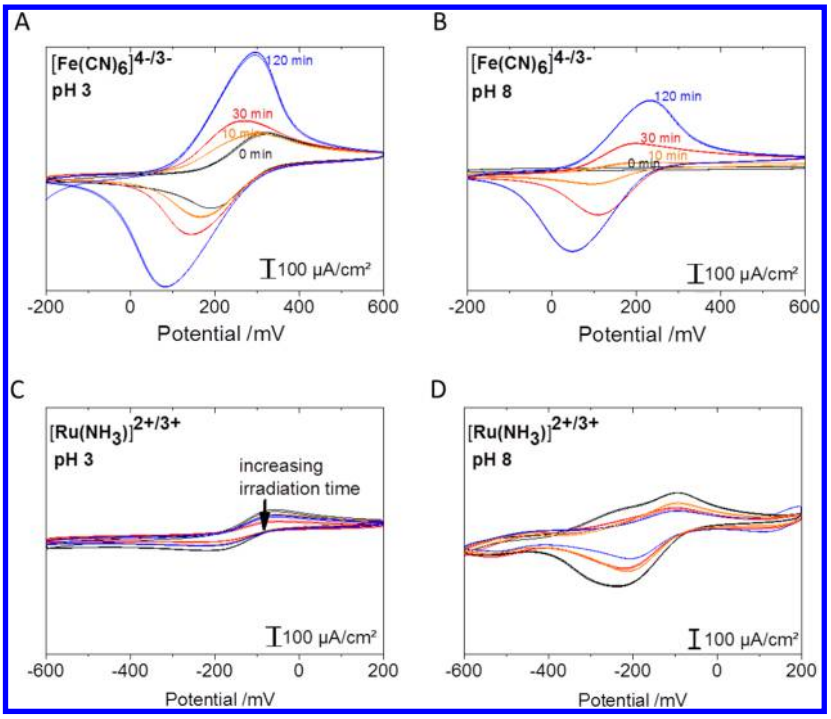

Figure 6. (A, B) Cyclic voltammetry response for the negatively charged probe molecule $[Fe(CN)_6]^{4-/3-}$ (***FC***) as a function of photopolymerization time: 0 min (black), 10 min (orange), 30 min (red), 120 min (blue) for pH 3 (A) and pH 8 (B). (C, D) Cyclic voltammetry response for the positively charged probe molecule $[Ru(NH_3)_6]^{2+/3+}$ (***RA***) in dependence of polymerization time: 0 min (black), 10 min (orange), 30 min (red), 120 min (blue) for pH 3 (C) and pH 8 (D), corresponding to Figure 6.

for pH above 4, a charge reversal is observed due to silanolate.[10,13,49]

For the maximum polymerization time explored of 210 min with respect to thermal ACVA initiation, which corresponds approximately to $n_{METAC}/n_{NH2} \sim 2$, signals for ***FC*** and ***RA*** are observed (Figure 5E). Additionally, the effect of the pH in the peak intensity is noticeably smaller than that in the amino silica film with $n_{METAC}/n_{NH2} = 0$. In the case of the negative probe, a voltammetric peak shift and slight broadening is observed at pH of 3. Peak broadening can be attributed to the electrostatic interactions between FC anions and PMETAC, as discussed above, while the peak shifts likely result from the effect of the acid−base equilibrium on the Donnan potential of the film.[50] The currents for FC are slightly lower for higher pH, indicating that a fraction of silanolate groups makes a small negative contribution to the surface charge, resulting in lower currents for the ***FC*** species. The corresponding voltammetric response of ***RA*** displayed in Figure 5E (right) shows that diffusion of the probe molecule takes place. Neither an exclusion, corresponding to a positively charged pore, nor a significant preconcentration, as expected for a negatively charged pore, are observed, such as, for example, for bare mesoporous silica. The results corresponding to the 210 min polymerization are very similar to those observed in the case of a polyelectrolyte-modified mesoporous silica surface, in which a charge-matching neutralizes the pores and permits the transport of charged species.[10] This suggests that the surface charge is practically neutralized by the PMETAC for $n_{METAC}/n_{NH2} \sim 2.3$.

The results for $t = 0$ min ($n_{METAC}/n_{NH2} = 0$) and $t = 210$ min ($n_{METAC}/n_{NH2} \sim 2.3$) demonstrate that the METAC amount within the mesopores can be controlled, leading to an increase of a positive charge within the pore system. The growth of PMETAC induces a permanent positive charge, and a decrease in the transport of positively charged molecules would be expected. However, the low average polymer amount achievable by thermal polymerization is not sufficient to reverse the silanolate-induced pore charge at basic pH.

For intermediate polymerization times, an increasing positive charge density corresponding to an increasing PMETAC content with increasing polymerization time is observed, confirming the results of DRIFT and pore-ellipsometry. In line with this observation, the transport of negatively charged ***FC*** constantly increases with increasing PMETAC content (Figure 5) for all pH conditions. For pH = 3 (slightly positive to neutral silica pore walls) the transport of ***FC*** is always higher than that for more basic pH (pore walls negatively charged) and increases starting from the j_p for 0 min polymerization, reaching a constant level after 120 min of polymerization ($n_{METAC}/n_{NH2} \sim 2.3$). The measured transport for the positively charged probe ***RA*** at pH 8 shows a decrease in the j_p signal for higher polymer content. The preconcentration of ***RA*** observed for the blank aminosilica films at pH > 5, due to the probe electrostatic adsorption onto silanolates, is reduced with increasing polymer content, resulting in j_p reproducing exactly the CV of bare ITO.

The observed facts are compatible with the interpretation that probe diffusion takes place in the pores, modulated by the pore surface charge. This charge is heavily influenced by the interplay of PMETAC contents and the silanolate species, which are in turn modified by pH. The complex observed behavior is completed by some contribution to the total current due to probe species interacting with the pore surface, either **RA** adsorbed on silanolate grops or **FC** preconcentrated by PMETAC, as a counterion. For PMETAC values of $n_{METAC}/n_{NH2} \sim 2.3$, a neutral pore is created, as already concluded from the transport results of the negative probe. For lower pH values, the interpretation is more complex. In the case of pH 3, when $n_{METAC}/n_{NH2} > 1$, the same trend is apparent, and j_p is

DOI: 10.1021/cm5037953
Chem. Mater. 2015, 27, 808−821

almost constant in the vicinity of $n_{METAC}/n_{NH2} = 2$, suggesting that even for those low polymer loadings the surface is nearly neutralized. For shorter residues (i.e., $n_{METAC}/n_{NH2} \sim 1$), the peak current density for ***RA*** increases when the average n_{METAC}/n_{NH2} increases, suggesting a complex transport mechanism arising from crossed charge and surface acidity effects, combined with pore wetting. At these low polymer loadings, unreacted amino groups or initiators might intervene on the surface charge. Further experiments are in due course to understand this behavior.

In summary, these results show a transformation of an aminosilica mesoporous film, which is slightly positively charged at pH 3 and negatively charged at pH > 5, into a neutral to slightly positively charged PMETAC-modified mesoporous film at pH 3, and a nearly neutral PMETAC-modified mesoporous film at pH > 5. It is worth noting that these effects were always measured under the conditions of intermediate ionic strength (100 mM KCl) and that variations of this parameter can also influence the electrostatic interactions and thus the perm-selective behavior.

Light-induced polymerization. Light-induced polymerization times were varied up to 120 min. Parts A and B of Figure 6 show the cyclic voltammograms for the negatively charged ***FC*** as a function of the polymerization time (black, 0 min; orange, 10 min; red, 30 min; blue, 120 min), and pH 3 or pH 8. As discussed above, the mesoporous aminosilica pore walls are slightly positively charged at pH 3, allowing the diffusion of the FC negative probe as indicated by the voltammetric response (Figure 6A, black, 0 min) whereas the cyclic voltammetry response changes appreciably for pH 8 (Figure 6B, black, 0 min), at which the mesopore walls are negatively charged and thus the negatively charged ***FC*** is excluded. For the maximum polymerization time of 120 min, a strong preconcentration of $[(Fe(CN)_6]^{3-}$ is evidenced by redox peaks that are much higher and broader than for the unmodified film and bare ITO-electrode. The detected j_p is also higher than for temperature-induced polymerization (Figure 5). The effect of the positive charged PMETAC is much more pronounced for pH 3, reflected in the higher j_p as compared to pH 8, indicating also an influence of the silanol/silanolate wall charge, as already discussed for the temperature-induced polymerization. The j_p for the negatively charged probe increases quickly with increasing polymerization time, which is in line with the higher polymer content and thus the higher charge content for the light-induced polymerization (Table 1). Plotting j_p against the square root of the scan rate results in a linear relationship, which strongly suggests that the electrochemical signal in our system is limited by diffusion.[41]

The voltammetric response of the positively charged ***RA*** for pH 3 (Figure 6C) shows diffusion of the probe molecule into the unmodified neutral membrane, and decreasing signal intensity with polymer being present until almost complete exclusion of the positive probe (Supporting Information), in excellent agreement with the results obtained for $[Fe(CN)_6]^{3-}$. Note the presence of two anodic peaks in the voltammograms of Figure 6D, which, as discussed above for thermal polymerization, we attribute to free and silanol bound RA probes. All evidence indicates that, for light-induced polymerization, an overall positively charged pore is obtained even for low polymerization times (10 min), after which $n_{METAC}/n_{NH2} > 5$ is achieved. Interestingly, even with these higher polymer contents the effect of pH and thus of the wall charge is still visible in the overall signal intensity (Figure 6C, D).

In summary, the results presented above show that the gradual incorporation of PMETAC into the pore space transforms an aminosilica mesoporous film with an approximate isoelectric point of 3−4 (i.e., slightly positively charged at pH 3, and negatively charged at pH > 5) into a neutral ($n_{METAC}/n_{NH2} < 5$) to clearly positively charged ($n_{METAC}/n_{NH2} > 5$) PMETAC-modified mesoporous film.

Modeling of the transport properties for mesoporous silica films with high PMETAC content. The experimental results discussed above suggest that the main factor determining the electrochemical response of the system is electrostatic preconcentration of the redox probe in the film. In a first approximation, therefore, we will ascribe the dependence of peak current with the degree of polymerization and pH to changes in the local concentration of the redox probe within the pore. We can, therefore, write

$$j_p/j_p^{ITO} = kC_{probe} \quad (2)$$

where k is a proportionality constant that we determine as a fitting parameter and assume to be independent of pH, n_{METAC}/n_{NH2}, and the identity of the redox probe. Note that this expression neglects the possible effect of the polymer on the mobility of the probe. However, we believe that the changes in mobility due to the introduction of the polymer will be less important than the changes in concentration. As we show below, the concentration of ionic species within the film can change by orders of magnitude upon PMETAC polymerization. We also neglect possible changes in the charge-transfer kinetics at the ITO electrode/film interface because, as shown above, the experimental evidence (Figure S2) indicates that the electrochemical response is limited by diffusional charge transport rather than by interfacial charge transfer.

In order to calculate C_{probe}, we used a previously developed molecular theory.[29,30] This theory considers explicitly the size, charge, charge distribution, and conformations of all chemical species in the system as well as the presence of coupled acid−base chemical equilibria. The outputs of the theory are the position-dependent concentration of the chemical species inside the pore (polymer, Cl^-, K^+, H^+, OH^-, redox probe), the electrostatic potential inside the pore, and the degree of dissociation of the ionizable groups on the pore inner walls (i.e., the silanol and amino groups). The Supporting Information contains a detailed derivation of the molecular theory for the current system and a description of the parameters of the model. In our calculations, we modeled the pores as cylinders of diameter d = 9 nm. The walls of the pore contain amino groups, silanol groups, and PMETAC chains grafted to amino groups. We set the total surface coverage of the amino groups to 0.9 nm^{-2} (this coverage includes both free amino groups and amino groups modified with PMETAC chains). The pK_a of the free amino groups was 10.0. Following literature references,[51,52] we considered two types of silanol groups with different acid−base properties: silanols Q3 (one silanol per silicon atom, $\sigma_{SiOH,Q3}$ = 0.72 nm^{-2} and pK_a = 2.0) and silanols Q2 (two silanols per silicon atom, $\sigma_{SiOH,Q2}$ = 2.88 nm^{-2} and pK_a = 8.2). The parameters required to model the polymer are the number of polymers per unit area (surface coverage, σ_P) and the degree of polymerization (N). The experimental characterization of the system provided us with an estimation of the ratio of METAC monomers per amino group, n_{METAC}/n_{NH2} (see above). However, we do not know whether each amino group has a PMETAC chain (which implies σ_P = 0.9 nm^{-2} and

DOI: 10.1021/cm5037953
Chem. Mater. 2015, 27, 808−821

$N = n_{METAC}/n_{NH2}$) or if there are amino groups that did not react during the anchoring of the initiator and thus are free (which leads to $\sigma_P < 0.9$ nm^{-2} and $N = n_{METAC}/n_{NH2} \times 0.9$ nm$^{-2}/\sigma_P$). We will assume here the first scenario (i.e., each amino group has a PMETAC chain). However, we show in the Supporting Information that the second scenario (i.e., only a fraction of amino groups has tethered chains) yields a transport behavior very similar to that reported here for the first scenario. Both scenarios produce similar results because, as was shown previously,[29] the factor determining the concentration of the redox probe inside the pore is the total number of METAC monomers ($N\cdot\sigma_P$) rather that the individual values of N or σ_P.

Figure 7a shows that the theory correctly predicts the increase of the ***FC*** current with n_{METAC}/n_{NH2} for both pH = 3

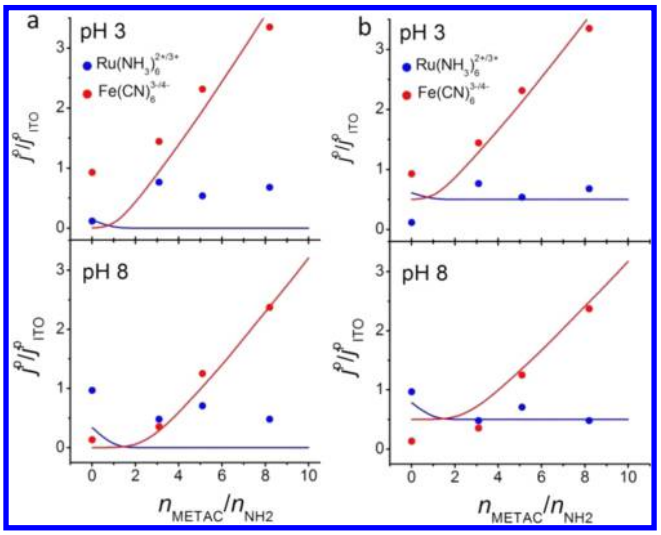

Figure 7. Comparison between experimental peak current densities (points) and predictions of the molecular theory (solid lines) as a function of the ratio of PMETAC segments to amino groups in the pore, n_{METAC}/n_{NH2}, for PMETAC brushes grown by light-induced polymerization. Panel **a** shows the predictions of eq 2, which considers the current arising from the probe molecules within the nanopores. Panel **b** shows the predictions of eq 3, which considers the current arising from probe molecules within the nanopores plus an additional nonpermselective parallel current.

and pH = 8. It also predicts correctly that the ***RA*** current remains constant as a function of n_{METAC}/n_{NH2}; however, it underestimates systematically the value of this current. In other words, the theory predicts an almost complete exclusion of ***RA*** for $n_{METAC}/n_{NH2} > 0$ and both pH = 3 and 8 due to the electrostatic repulsions between the positively charged PMETAC chains and the highly charge $Ru(NH_3)_6^{3+}$ probe. However, we observe a non-negligible Ru peak current in the experiments. We propose that this discrepancy can be explained by the presence of a nonpermselective path of ion transport in the system (i.e., a nonpermselective parallel current). We thus modified our model in order to account for this non-permselective current:

$$j_p/j_p^{ITO} = kC_{probe} + J \quad (3)$$

where J is a fitting parameter independent of n_{METAC}/n_{NH2}, pH, and type of probe. Figure 7b shows that the inclusion of the nonpermselective parallel current greatly improves the agreement between theory and experiment. Our theory captures the transport properties of the system for both types of redox probes, two different pH values, and different values of n_{METAC}/n_{NH2} using only two fitting parameters (k and J). The origin of the parallel current may involve imperfections in the film, or adsorption of electroactive species on the pore surface, leading to a second path for electrons; ongoing work is investigating these possibilities.

The molecular theory makes predictions on the distribution of all species in the system, providing important insights on the molecular organization within the pore. Figure 8 shows the

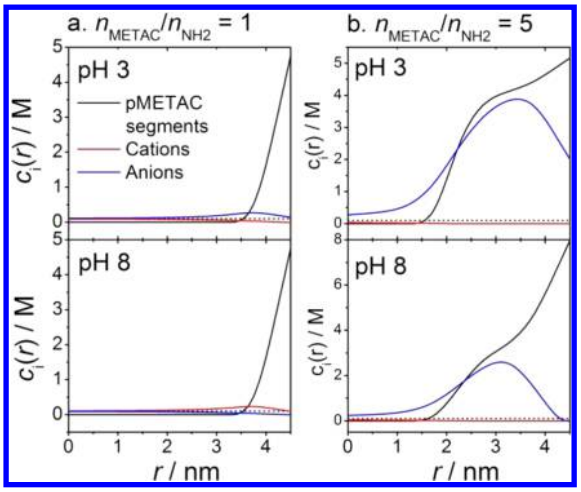

Figure 8. Molar concentration of polymer segments, cations (K^+) and anions (Cl^-), as a function of the distance from the center of the pore, r, as predicted by the molecular theory calculations. The dashed line shows the bulk concentration of KCl (c^{bulk} = 0.1 M). The small concentration of the redox probes is not shown in this plot.

number density of anions, cations, and polymer segments as a function of the distance from the center of the pore, r (r = 0 corresponds to the center of the pore) for pH = 3 and 8 and n_{METAC}/n_{NH2} = 1 and 5. Since we assumed that every amino group has a tethered PMETAC chain in the calculations, the conditions n_{METAC}/n_{NH2} = 1 and 5 imply chains lengths, N, of 1 and 5, respectively. In all cases, the theory predicts that the density of the polymer is maximum at the surface of the pore due to the electrostatic attraction between the METAC monomers and the silanol groups on the walls. Therefore, the positive polyelectrolyte collapses to the walls of the pore in order to neutralize its charge, even when this process results in a loss of configurational entropy.

For n_{METAC}/n_{NH2} = 1 and pH 8, the positive charge of the polymer is smaller than the negative charge of the wall and, thus, the concentration of K^+ cations is slightly enhanced within the pore and the concentration of Cl^- anions is depleted (cation permselective system). In all other cases shown in Figure 8, the charge of the polymer plus the charge of the wall is positive; hence, those systems exhibit anion permselectivity. Note that, for pH 8, the pore is selective to cations for n_{METAC}/n_{NH2} = 1 and to anions for n_{METAC}/n_{NH2} = 5. The theory predicts that transition between anion and cation permselectivity occurs for $n_{METAC}/n_{NH2} \sim 1.5$.

The combination of experiments and theory shows that ionic perm-selectivity in mesoporous hybrid thin films can be adjusted gradually by adjusting polyelectrolyte content, either by changing the polymerization method or by varying the polymerization time. As sketched in Figure 9, three regions can be clearly determined for both acidic and alkaline media: (a)

DOI: 10.1021/cm5037953
Chem. Mater. 2015, 27, 808−821

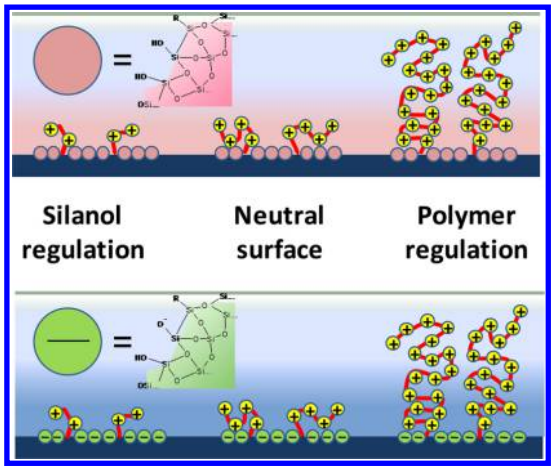

Figure 9. Schematic summary of the behavior of the polymer-modified silica surface. The upper scheme represents acidic conditions (pH < 3) in which the surface is covered with silanol or protonated silanol groups. The lower figure represents alkaline media (pH > 7), presenting silanolate surface groups. The polymerization degree, *N*, increases from left to right; regions of different charge control regime are indicated.

n_{METAC}/n_{NH2} < 2 (i.e., an occupied pore volume of *F*% < 25%), in which a combination of the surface charge modulated by the silanols, residuals of amino/ammonium functions, and some METAC groups are responsible for the selective transport of ions, depending on pH (i.e., the system is selective to cations at high pH and to anions at low pH), (b) n_{METAC}/n_{NH2} ~2−5, with neutralized pores through which transport of cations or anions can take place, and no exclusion is observed, (c) n_{METAC}/n_{NH2} > 5, in which the transport of cations dramatically decreases, and anion transport or preconcentration can be controlled. However, the observed behavior is more complex and smaller residual non perm-selective currents can be due to interfacial effects such as adsorption.

The control processes shown here open new paths to pattern transport from exclusion to preconcentration of charged molecules by selecting the appropriate polymerization strategy and polymerization parameters. Interestingly, pore volume effects do not seem to play a central role; this may be due to a compensation between preconcentration and volume reduction effects. In addition, the access of anions into a pore that is completely filled by polymer suggests that the polymer is permeable to the ions *per se* and the ion transport is mostly controlled by electrostatic factors.

CONCLUSIONS

In this work we demonstrate that free radical polymerization by thermal or light-induced activation is a feasible route for the controlled production of PMETAC inside mesoporous membranes. A gradual tuning of polymer content within the mesopores can be achieved by adjusting the used initiator and the polymerization time. Increasing polymerization time results in increasing polymer content and thus increasing positive charge inside the nanoconfined pores, as was proved by DRIFT and ellipsometric porosimetry. This strategy of adjustment of charge density allows the tuning of ionic permselectivity of charged probe molecules such as $[Fe(CN)_6]^{4-/3-}$ and $[Ru(NH_3)_6]^{2+/3+}$ through the hybrid membrane. Three regions have been identified with different tunable permeability. For low PMETAC contents, transport is controlled by surface silanolates, resulting in a membrane preconcentrating positively charged molecules while excluding negatively charged ones. Reaching a PMETAC content of *F*% > 25% occupied pore volume (n_{METAC}/n_{NH2} ~ 2.3) results in a neutral pore, allowing the diffusion of positively and negatively charged molecules. This experimental result is in very good agreement with our theoretical model that predicts charge neutralization for n_{METAC}/n_{NH2} ~ 1.5. A further increase of PMETAC content creates a positively charged pore starting to preconcentrate the negative probe $[Fe(CN)_6]^{4-/3-}$ and hindering the transport of positive molecules such as $[Ru(NH_3)_6]^{2+/3+}$. Nevertheless, in all cases permselectivity was influenced by the solution pH. Even for PMETAC contents of n_{METAC}/n_{NH2} > 5 the deprotonation of the pore wall silanolate groups reduced the preconcentration of $[Fe(CN)_6]^{4-/3-}$. This shows that already low amounts of polymer significantly change the behavior of mesoporous membranes, but the pore wall maintains an influence on the observed permselectivity. Such a gradual tuning of transport characteristics from exclusion to preconcentration shows the utmost importance of charge density control to manipulate transport.

Central to the ability of controlling pore gating is the identification of the driving forces toward perm-selectivity. From our CV studies, it is clear that a combination of electrostatic and steric effects controls the pore permeability and the mechanisms of probe permeation. While more detailed studies are needed in order to completely understand the effects of diffusion and preconcentration, it is clear that controlling the pore volume and surface charge by the tuned addition of a polyelectrolyte is a valid route toward building intelligent nanopores.

Fundamental understanding will also require improving our theoretical tools. In this work, we used a theory to model the molecular environment within the mesopores. We then used fitting parameters to relate the concentration of the redox probes within the film predicted by this theory with the electrochemical response as a function of pH and degree of polymerization. This approach to study the electrochemical response is rather indirect, as it neglects the details of the diffusional fluxes in the system. Future theoretical models will extend this methodology to incorporate a description of the diffusional processes in the system, allowing truly predictive simulations of the electrochemical response, without losing molecular detail.

The possibility of using different polymerization strategies to control polymer content or macroscopic positioning opens a variety of new paths for transport tuning, and should be applicable to a wide variety of hybrid membrane systems integrated in lab-on-chip or electronic devices. In addition, the possibilities of controlling the polymer loading within a mesopore by irradiation opens interesting avenues in the lithographic patterning of mesoporous materials for microfluidics.

ASSOCIATED CONTENT

Supporting Information

Characterization details, fluorescence microscope images, j_p vs scan rate plots, water adsorption isotherms (left) and neck size distributions (right), and derivation of the molecular theory. This material is available free of charge via the Internet at http://pubs.acs.org.

DOI: 10.1021/cm5037953
Chem. Mater. 2015, 27, 808−821

AUTHOR INFORMATION

Corresponding Authors

*E-mail: brunsen@cellulose.tu-darmstadt.de (AB) .
*E-mail: gsoler@cnea.gov.ar (GJAASI).

Notes

The authors declare no competing financial interest.

ACKNOWLEDGMENTS

We gratefully acknowledge financial support from the Landesoffensive zur Entwicklung Wissenschaftlich-ökonomischer Exzellenz (LOEWE Soft Control) Agencia Nacional de Promoción Científica y Tecnológica (ANPCyT) (PICT 1848 and 2087, PAE 2004 22711, PICT 2010-457, and PICT-PRH 163/08), Centro Interdisciplinario de Nanociencia y Nanotecnología (CINN, PAE 2006 37063, projects PRH 2007-74, PIDRI no. 74, and PME 00038), Fundación Petruzza, Gabbos (DG-017), Max-Planck-Gesellschaft (Max Planck Partner Group – MPIP/INIFTA), Consejo Nacional de Investigaciones Científicas y Técnicas (CONICET, PIP 11220100100186), Alexander von Humboldt Stiftung, Laboratorio Nacional de Luz Sincrotron (LNLS) (XRD2-11639/10736; SXS-11642), and Universidad de Buenos Aires (UBACYT 2010-2012, Grant No.: 20020090100164). G.J.A.A.S.-I. and O.A. are CONICET fellows. Prof. Katja Schmitz (Technische Universität Darmstadt) is gratefully acknowledged for support in fluorescence microscopy. We especially thank Fabio Krohm, as well as Ulrike Kunz and Prof. Kleebe from the Material Science Department of the Technical University Darmstadt, for their support with TEM measurements. I.S. acknowledges the National Science Foundation of USA for support under grant CBET-1403058.

REFERENCES

(1) Huber, D. L.; Manginell, R. P.; Samara, M. A.; Kim, B. I.; Bunker, B. C. *Science* **2003**, *301*, 352−354.
(2) Choi, M.; Kleitz, F.; Liu, D.; Lee, H. Y.; Ahn, W.-S.; Ryoo, R. *J. Am. Chem. Soc.* **2005**, *127*, 1924−1932.
(3) Soler-Illia, G. J. A. A.; Azzaroni, O. *Chem. Soc. Rev.* **2011**, *40*, 1107−1150.
(4) Schoch, R. B.; Han, J.; Renaud, P. *Rev. Modern Phys.* **2008**, *80*, 839−883.
(5) Mann, S.; Ozin, G. A. *Nature* **1996**, *382*, 313.
(6) Sanchez, C.; Arribart, H.; Guille, M. M. G. *Nat. Mater.* **2005**, *4*, 277−288.
(7) Rohlfing, D. F.; Rathouský, J.; Rohlfing, Y.; Bartels, O.; Wark, M. *Langmuir* **2005**, *21*, 11320−11329.
(8) Fattakhova-Rohlfing, D.; Wark, M.; Brezesinski, T.; Smarsly, B. M.; Rathouský, J. *Adv. Funct. Mater.* **2007**, *17*, 123−132.
(9) Calvo, A.; Angelome, P. C.; Sanchez, V. M.; Scherlis, D. A.; Williams, F. J.; Soler-Illia, G. J. A. A. *Chem. Mater.* **2008**, *20*, 4661−4668.
(10) Brunsen, A.; Calvo, A.; Williams, F. J.; Soler-Illia, G. J. A. A.; Azzaroni, O. *Langmuir* **2011**, *27*, 4328−4333.
(11) Calvo, A.; Yameen, B.; Williams, F. J.; Azzaroni, O.; Soler-Illia, G. J. A. A. *Chem. Commun.* **2009**, 2553−2555.
(12) Calvo, A.; Fuertes, M. C.; Yameen, B.; Williams, F. J.; Azzaroni, O.; Soler-Illia, G. J. A. A. *Langmuir* **2010**, *26*, 5559−5567.
(13) Calvo, A.; Yameen, B.; Williams, F. J.; Soler-Illia, G. J. A. A.; Azzaroni, O. *J. Am. Chem. Soc.* **2009**, *131*, 10866−10868.
(14) Brunsen, A.; Díaz, C.; Pietrasanta, L. I.; Yameen, B.; Ceolín, M.; Soler-Illia, G. J. A. A.; Azzaroni, O. *Langmuir* **2012**, *28*, 3583−3592.
(15) Brunsen, A.; Cui, J.; Ceolín, M.; Campo, A. D.; Soler-Illia, G. J. A. A.; Azzaroni, O. *Chem. Commun.* **2012**, *48*, 1422−1424.
(16) Jung, Y. S.; Sun, Z.; Wuenschell, J.; Kim, H. K.; Kaur, P.; Wang, L.; Waldeck, D. *Appl. Phys. Lett.* **2006**, *88*, 35.
(17) Zhao, B.; Brittain, W. J. *Prog. Polym. Sci.* **2000**, *25*, 677−770.
(18) Pyun, J.; Kowalewski, T.; Matyjaszewski, K. *Macromol. Rapid Commun.* **2003**, *24*, 1043−1059.
(19) Edmondson, S.; Osborne, V. L.; Huck, W. T. S. *Chem. Soc. Rev.* **2004**, *33*, 14−22.
(20) Boyes, S. G.; Granville, A. M.; Baum, M.; Akgun, B.; Mirous, B. K.; Brittain, W. J. *Surf. Sci.* **2004**, *570*, 1−12.
(21) Jennings, G. K.; Brantley, E. L. *Adv. Mater.* **2004**, *16*, 1983−1994.
(22) Rühe, J.; Ballauf, M.; Biesalski, M.; Dziezok, P.; Grohn, F.; Johannsmann, D.; Houbenov, N.; Hugenberg, N.; Konradi, R.; Minko, S.; Motornov, M.; Netz, R. R.; Schmidt, M.; Seidel, C.; Stamm, M.; Stephan, T.; Usov, D.; Zhang, N. H. *Adv. Polym. Sci.* **2004**, *165*, 79−150.
(23) Tsujii, Y.; Ohno, K.; Yamamoto, S.; Goto, A.; Fukuda, T. *Adv. Polym. Sci.* **2006**, *197*, 1−45.
(24) Kruk, M.; Dufour, B.; Celer, E. B.; Kowalewski, T.; Jaroniec, M.; Matyjaszewski, K. *Macromolecules* **2008**, *41*, 8584−8591.
(25) Krohm, F.; Didzoleit, H.; Schulze, M.; Dietz, C.; Stark, R. W.; Hess, C.; Stühn, B.; Brunsen, A. *Langmuir* **2014**, *30*, 369−379.
(26) Schepelina, O.; Zharov, I. *Langmuir* **2008**, *24*, 14188−14194.
(27) Huang, W.; Skanth, G.; Baker, G. L.; Bruening, M. L. *Langmuir* **2001**, *17*, 1731.
(28) Wei, X.; Ngai, T. *Polym. Chem.* **2012**, *3*, 2121−2128.
(29) Tagliazucchi, M.; Azzaroni, O.; Szleifer, I. *J. Am. Chem. Soc.* **2010**, *132*, 12404−12411.
(30) Tagliazucchi, M.; Calvo, E. J.; Szleifer, I. *J. Phys. Chem. C* **2008**, *112*, 458−471.
(31) Fattakhova-Rohlfing, D.; Wark, M.; Rathousky, J. *Chem. Mater.* **2007**, *19*, 1640−1647.
(32) Calvo, A.; Joselevich, M.; Soler-Illia, G. J. A. A.; Williams, F. J. *Microporous Mesoporous Mater.* **2009**, *121*, 67−72.
(33) Barth, A. *Biochim. Biophys. Acta* **2007**, *1767*, 1073−1101.
(34) Nicole, L.; Boissière, C.; Grosso, D.; Quach, A.; Sanchez, C. *J. Mater. Chem.* **2005**, *15*, 3598−3627.
(35) Boissiere, C.; Grosso, D.; Lepoutre, S.; Nicole, L.; Bruneau, A. B.; Sanchez, C. *Langmuir* **2005**, *21*, 12362−12371.
(36) Zhuravlev, L. T. *Colloid Surf., A: Physicochem. Eng. Aspects* **2000**, *173*, 1−38.
(37) Cao, L. A.; Kruk, M. *Polym. Chem.* **2010**, *1*, 97−101.
(38) Kobayashi, M.; Terayama, Y.; Hino, M.; Ishihara, K.; Takahara, A. *Journal of Physics: Conference Series* **2009**, *184*, 012010.
(39) Amatore, C.; Oleinick, A.; Klymenko, A. V.; Delacote, C.; Walcarius, A.; Svir, I. *Anal. Chem.* **2008**, *80*, 3229−3243.
(40) Amatore, C. *Chem.—Eur. J.* **2008**, *14*, 5449−5464.
(41) Bard, A. J.; Faulkner, L. R. *Electrochemical Methods: Fundamentals and Applications*; John Wiley and Sons: New York, 2000.
(42) Walcarius, A.; Kuhn, A. *Trends Anal. Chem.* **2008**, *27*, 593.
(43) Etienne, M.; Quach, A.; Grosso, D.; Nicole, L.; Sanchez, C.; Walcarius, A. *Chem. Mater.* **2007**, *19*, 844−856.
(44) Rafti, M.; Brunsen, A.; Fuertes, M. C.; Azzaroni, O.; Soler-Illia, G. J. A. A. *ACS Appl. Mater. Interface* **2013**, *5*, 8833−8840.
(45) Calvo, A. *Films Delgados mesoporosos híbridos conteniendo el grupo amino: una plataforma para el diseño y producción de membranas permeoselectivas*. PhD. Thesis, Universidad de San Martín, 2010.
(46) Walcarius, A.; Etienne, M.; Lebeau, B. *Chem. Mater.* **2003**, *15*, 2161−2173.
(47) Taffa, D. H.; Kathiresan, M.; Walder, L.; Seelandt, B.; Wark, M. *Phys. Chem. Chem. Phys.* **2010**, *12*, 1473−1482.
(48) Otal, E. H.; Angelomé, P. C.; Bilmes, S. A.; Soler-Illia, G. J. A. A. *Adv. Mater.* **2006**, *18*, 934−938.
(49) Elbert, J.; Krohm, F.; Rüttiger, C.; Kienle, S.; Didzoleit, H.; Balzer, B. N.; Hugel, T.; Stühn, B.; Gallei, M.; Brunsen, A. *Adv. Funct. Mater.* **2014**, *24*, 1591−1601.
(50) Tagliazucchi, M.; Williams, F. J.; Calvo, E. J. *J. Phys. Chem. B* **2007**, *111*, 8105−8113.
(51) Rosenholm, J. M.; Czuryszkiewicz, T.; Kleitz, F.; Rosenholm, J. B.; Lindén, M. *Langmuir* **2007**, *23*, 4315−4323.

DOI: 10.1021/cm5037953
Chem. Mater. 2015, 27, 808−821

(52) Ong, S. W.; Zhao, X. L.; Eisenthal, K. B. *Chem. Phys. Lett.* **1992**, *191*, 327−335.

DOI: 10.1021/cm5037953
Chem. Mater. 2015, 27, 808−821